Pergamon

Cement and Concrete Research 29 (1999) 377–387

CEMENT AND CONCRETE RESEARCH

Immittance spectra for Portland cement/fly ash-based binders during early hydration[1]

W.J. McCarter *, G. Starrs, T.M. Chrisp

Department of Civil and Offshore Engineering, Heriot-Watt University, Edinburgh, EH14 4AS, Scotland, UK

Manuscript received 19 August 1998; accepted manuscript 3 November 1998

Abstract

A range of immittance formalisms is exploited to understand the nature of conduction and polarization within Portland cement-based binders over the frequency range 1 Hz to 1 MHz. Data are presented for binders with and without aggregate additions; of particular interest was the electrical response of a binary combination of ordinary Portland cement and fly ash. Regarding the latter, when presented on a Nyquist diagram, a characteristic plateau region emerged between the electrode spur and the bulk arc. When presented in the form of dielectric constant and conductivity as a function of frequency, a region of dispersion was evident for all systems. Furthermore, it was shown that by undertaking a dielectric frequency-domain analysis of the data, the experimental results could be synthesized across the frequency range 1 kHz to 1 MHz. Rather than ascribing separate processes to each impedance zone, the observed response could be attributed to a single bulk polarization process. When transformed into the complex impedance plane, there was also good agreement between synthesized and measured response. It is postulated that polarization is as a result of double-layer effects on the grain with a relaxation frequency in the low kilohertz region.

Keywords: Fresh concrete; Characterization; Electrical properties; Fly ash

Since its initial application to Portland cement paste [1], a considerable amount of work has now been published on the application of alternating current (a.c.) impedance spectroscopy in characterising microstructural evolution and pore structure development in cement-based systems [2–16]. Much of this work, however, has concentrated on neat cement pastes and mortars, with attention being directed towards the later stages of hydration, i.e., during the hardening process. In comparison, only limited studies have been undertaken on cement pastes [5,17,18], mortars, and concretes [18–20] during the very early stages of hydration, i.e., before setting.

When plotted in Nyquist format, the impedance response of ordinary Portland cement (OPC) concretes and mortars [18–20], before setting, has revealed a two-region response over the frequency range 1 Hz to 15 MHz, although data are severely degraded at the higher frequencies. This is not dissimilar to that obtained from hardened cementitious systems with the regions comprising a low-frequency spur attributed to electrode effects and a high-frequency depressed arc associated with bulk processes. It also was shown in this work that when OPC binder is partially replaced by fly ash (FA), a characteristic three-region response is obtained: a low-frequency spur ($<$1 kHz), a mid-frequency plateau region ($\approx$1–150 kHz), and a high-frequency bulk arc ($>$150 kHz). The extent and prominence of the plateau region were shown to vary with the level of FA replacement, becoming more evident with increasing replacement level. This could be of considerable practical significance as a means of detecting and quantifying the amount of FA in a freshly batched concrete mix, hence exploited as a technique in the quality control of such concretes. In the design of high-performance cementitious systems, FA has a role to play and quality control is essential at all stages of their production to ensure the requirements of function and durability.

These previous studies are limited in a number of respects, particularly in the format of data presentation, the lack of electrical modelling of the experimental data, and detail on the underlying mechanisms responsible for conduction and polarization in OPC-based binders. Regarding the former, we believe that the common approach of fitting equivalent circuit models separately to each of the regions noted earlier is not necessarily the best method for revealing

* Corresponding author. Tel.: 44-131-451-3143; Fax: 44-131-3170/5078; E-mail: johnm@civ.hw.ac.uk.

[1] This paper was originally submitted to Advanced Cement Based Materials. The paper was received at the Editorial Office of Cement and Concrete Research on 19 August 1998 and accepted in final form on 3 November 1998.

0008-8846/99/$–see front matter
PII: S0008-8846(98)00209-9

the underlying effects responsible for the observed impedance response. The work presented addresses these issues together with new data on electrical measurements of fresh cement-based systems.

1. Immittance spectroscopy

The intrinsic electrical properties of any nonmagnetic material can be fully specified by the frequency-dependent parameters dielectric constant, $\varepsilon_r'(\omega)$, and conductivity, $\sigma(\omega)$. These are determined by the polarization and conduction of bound and free charges within the material. If the material is heterogeneous, $\varepsilon_r'(\omega)$ and $\sigma(\omega)$ will be strongly correlated to the properties of the individual components and the way in which they are combined. Such correlation is often manifested in the frequency domain as dispersive behavior characterised by frequencies of relaxation, above which dielectric constant falls and conductivity rises. Therefore, it can be possible to identify various features of heterogeneous materials by their electrical properties, provided they are observed over a wide enough frequency range (immittance spectroscopy). The term immittance covers several levels of response that can be obtained by a.c. electrical measurements: relative permittivity $\varepsilon_r(\omega)$ and its reciprocal electric modulus $M(\omega)$; impedance $Z(\omega)$ and its reciprocal admittance $Y(\omega)$ [21]. The current work focuses on the impedance and permittivity levels.

Impedance, in a two-terminal a.c. system, is the frequency-domain ratio of applied voltage to resultant current. As such, it is a frequency-dependent complex parameter and normally is given in rectangular form as given in Eq. (1):

$$Z(\omega) = Z'(\omega) - jZ''(\omega) \text{ ohm } (\Omega) \tag{1}$$

where j is the complex operator $\sqrt{-1}$, ω is radian frequency (rad/s), the real part $Z'(\omega)$ is the resistive component, and the imaginary part $Z'(\omega)$ is the reactive component. Impedance is commonly presented graphically in Nyquist form, where $-Z''(\omega)$ is plotted against $Z'(\omega)$ over several decades of frequency. In the case of a measurement cell consisting of a lossy dielectric material (i.e., partly conducting) placed between a pair of parallel-plate electrodes, the relationship between the intrinsic electrical properties and the cell impedance is given in Eq. (2):

$$Z(\omega) = \frac{1}{(j\omega\varepsilon_0\varepsilon_r)(A/d)} \tag{2}$$

where A is the electrode surface area (m^2), d is the electrode separation (m), ε_0 is the permittivity of free space (8.854×10^{-12} F/m), and ε_r is the relative permittivity of the material. Relative permittivity is, itself, a frequency-dependent complex quantity comprising the dielectric constant, ε_r' and the dielectric loss ε_r'', related by Eq. (3):

$$\varepsilon_r(\omega) = \varepsilon_r'(\omega) - j\varepsilon_r''(\omega). \tag{3}$$

The dielectric constant accounts for energy storage resulting from the polarization of charges within the material, and the loss factor accounts for the dissipation of energy incurred in the polarization process together with any direct transfer of charge through the material. The effects of loss also may be represented as a conductivity, $\sigma(\omega)$, which is related to ε_r'' by Eq. (4):

$$\varepsilon_r''(\omega) = \frac{\sigma(\omega)}{\omega\varepsilon_0}. \tag{4}$$

Conductivity can result from both direct (ionic) conduction processes and dissipative polarization processes [22]. However, if the sample material has a known value of direct current (d.c.) (or low-frequency) ionic conductivity, it may be desirable to express the effects of ionic conduction separately to purely dielectric dissipative effects, in which case, as given in Eq. (5):

$$\sigma(\omega) = \sigma_d(\omega) + \sigma(0) \tag{5}$$

where $\sigma(0)$ is the d.c. ionic conductivity, and $\sigma_d(\omega)$ the dielectric conductivity. In this case, the relative permittivity can be more specifically given as in Eq. (6):

$$\varepsilon_r(\omega) = \varepsilon_r'(\omega) - j\left(\varepsilon_r''(\omega) + \frac{\sigma(0)}{\omega\varepsilon_0}\right). \tag{6}$$

The behavior of both dielectric constant and conductivity in the frequency domain will be determined by the polarization mechanisms from which they arise. According to the classic approach of Debye, the dispersion of the relative permittivity resulting from a single polarization mechanism can be described by Eq. (7) [22]:

$$\varepsilon_r = \varepsilon_{r\infty} + \frac{\varepsilon_{rs} - \varepsilon_{r\infty}}{(1 + (j\omega\tau_o)^{(1-\alpha)})} \tag{7}$$

where τ_o is the relaxation time-constant of the process (relaxation frequency is $\omega_o = 1/\tau_o$ radians/s), ε_{rs} is the dielectric constant of the material as ω approaches low frequencies (i.e., $\omega << \omega_o$), and $\varepsilon_{r\infty}$ is the dielectric constant as ω approaches high frequencies ($\omega >> \omega_o$). The exponent α ($0 < \alpha < 1$) is a dispersion factor that is included to account for the statistical distribution of relaxation times about a mean value of τ_o, which often is observed in real dielectrics. Separation of the real and imaginary parts of Eq. (7) and comparison with Eqs. (3) and (4) yields Eqs. (8A) and (8B) for dielectric constant and conductivity:

$$\varepsilon_r'(\omega) = \varepsilon_{r\infty} + \frac{(\varepsilon_{rs} - \varepsilon_{r\infty})\left[1 + (\omega\tau_o)^{(1-\alpha)}\sin\left(\alpha\frac{\pi}{2}\right)\right]}{\left(1 + (\omega\tau_o)^{2(1-\alpha)} + \left[2(\omega\tau_o)^{(1-\alpha)}\sin\left(\alpha\frac{\pi}{2}\right)\right]\right)} \tag{8A}$$

$$\sigma(\omega) = \varepsilon_{r\infty} + \frac{\omega\varepsilon_o(\varepsilon_{rs} - \varepsilon_{r\infty})\left[(\omega\tau_o)^{(1-\alpha)}\cos\left(\alpha\frac{\pi}{2}\right)\right]}{\left(1 + (\omega\tau_o)^{2(1-\alpha)} + \left[2(\omega\tau_o)^{(1-\alpha)}\sin\left(\alpha\frac{\pi}{2}\right)\right]\right)}. \tag{8B}$$

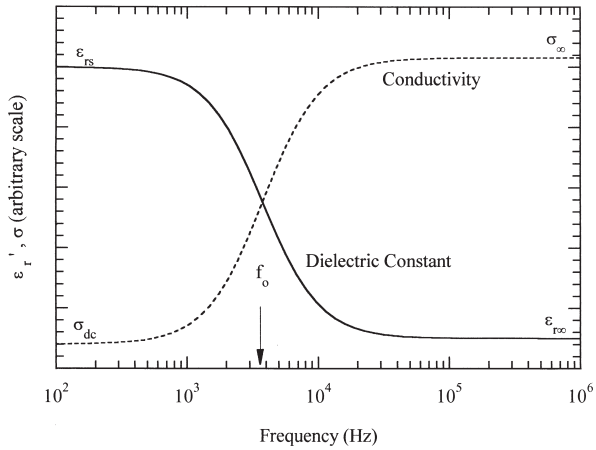

Fig. 1. Idealised dielectric and conductivity dispersion curves for a single relaxation process ($\alpha = 1$).

When $\alpha \rightarrow 0$, the terms in square brackets disappear and the resulting response has the form shown in Fig. 1. In a heterogeneous material (such as concrete, mortar, or cement paste), several superimposed relaxation mechanisms could be operating simultaneously. Each of these will make its own contribution to the bulk dielectric constant and will relax in accordance with its own time constant. If these are sufficiently disparate for each mechanism, then the individual features of the overall response will be discernible in the frequency domain.

The relationship between the response at the impedance level and that at the intrinsic permittivity level is illustrated in Figs. 2A and 2B. These plots were produced by means of Eqs. (2), (6), and (7), using theoretical data generated from the response of an equivalent circuit consisting of two parallel capacitor-resistor (C-R) networks connected in series. The resistances used were each 50 Ω, and the capacitances were 2 μF and 20 nF. It is noteworthy that while the impedance level response indicates two impedance relaxation frequencies at 1.48 and 145.3 kHz, the response at the intrinsic permittivity level has only one relaxation frequency at 3.5 kHz. If such a response was obtained from a real material, it could, therefore, be a mistake to interpret relaxations occurring in the impedance plane as intrinsic dielectric relaxations. Also, in this and other simulations, we found no simple or direct relationship between the value of the impedance level relaxation frequencies and that occurring at the permittivity level.

To develop an understanding of the mechanisms responsible for the impedance behaviour, we considered it more informative to present data in the form of dielectric constant and conductivity plotted as a function of frequency as per Fig. 1, as well as in the more common impedance format.

1. Experimental

1.1. Materials and sample preparation

Table 1 presents the mix proportions for the pastes, mortars, and concretes used in the present study. The binder comprised a blend of OPC (British Standard (BS) 12:1991; ASTM type I) and FA (BS3892: Part 1:1993; ASTM class F) at replacement levels of 10%, 25%, and 40% (by mass). For comparative purposes, tests were undertaken on specimens made from sulfate-resisting Portland cement (SRPC to BS4027: 1980; ASTM type V) and microsilica (MS) and noted on Table 1. Table 2 presents the physical and chemical properties of the OPC, FA, and MS. The fine and coarse aggregates were crushed rock, the coarse aggregate was prepared from two single size fractions, 5–10 mm and 10–20 mm, blended at a ratio of 1:2.

A 10-dm^3 Hobart planetary motion mixer was used for preparation of paste and mortar samples; a 0.1-m^3 pan mixer was used for preparation of concrete samples. All materials were dry mixed for approximately 30 s before gauging with water, and then mixed for a further 2 min before compaction into the test cells (described later) in two layers. The sample surface was smoothed level with the top of the cell, which then was connected to the frequency response analyser

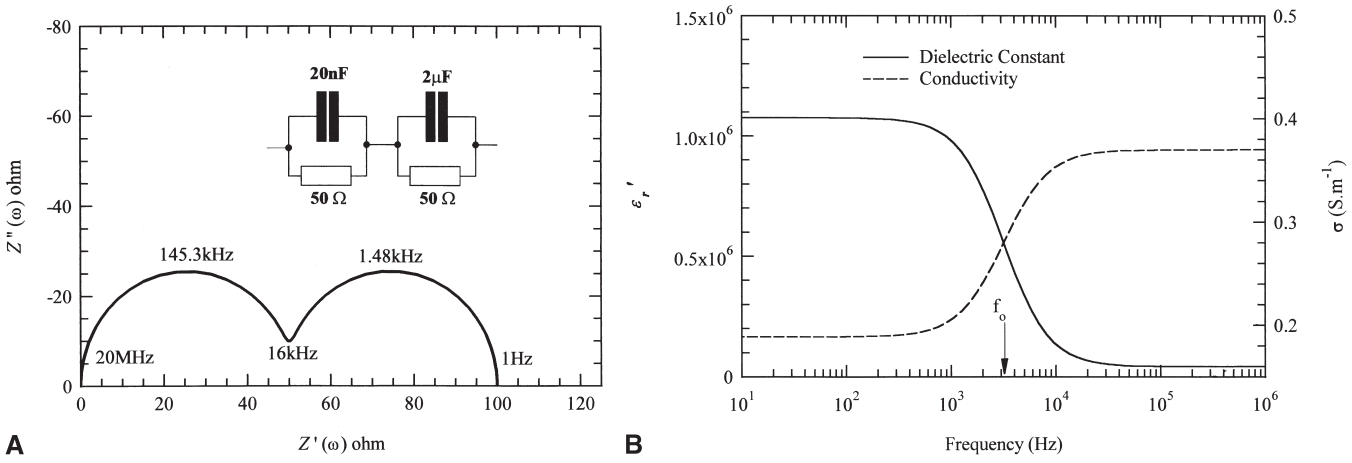

Fig. 2. *(A)* Calculated complex impedance curve for circuit indicated. *(B)* Calculated dielectric constant and conductivity dispersion curves for the same circuit.

Table 1
Summary of mixes studied

Mix	OPC (kg/m^3)	PFA (kg/m^3)	Fine (kg/m^3)	Coarse (kg/m^3)	Water (1/m^3)	Comments
P1	1619	—	—	—	485	
P2	1421	158	—	—	474	
P3	1141	380	—	—	456	
P4	881	587	—	—	440	
P5	1415	—	—	—	472	MS: 157 kg/m^3
M1	475	—	1425	—	310	
M2	425	47	1420	—	307	
M3	350	118	1330	—	304	
M4	277	185	1385	—	300	
M5	500	—	1500	—	275	SRPC
M6	368	122	1470	—	270	SRPC
M7	426	—	1420	—	307	MS: 47 kg/m^3
C1	405	—	608	1217	183	
C2	363	40	605	1209	181	
C3	300	100	600	1200	180	
C4	237	158	593	1186	178	

(FRA). All tests were carried out in a temperature controlled environment at 21 ± 1°C.

1.2. Electrical measurements and test cells

Impedance data were acquired using the Solartron 1260 FRA in voltage drive mode using a logarithmic sweep over the frequency range 1 Hz to 10 MHz. The signal voltage was optimised at 100 mV and the data were recorded at 100 points within the frequency range.

Samples were contained in rigid plexiglass cells of internal dimensions 50 × 50 × 50 mm for paste and mortar specimens, and 150 × 150 × 150 mm for the concrete specimens. Attached to two opposite sides of the cells were 3-mm thick, stainless-steel parallel-plate electrodes measuring 50 × 50 mm and 150 × 150 mm, respectively. These sides were demountable to facilitate removal of the sample. The cell sizes were considered sufficiently large to enable the acquisition of impedance measurements representative of bulk properties not distorted by localised heterogeneties. Stainless-steel connections were passed through the cell walls and secured to the electrodes to facilitate electrical contact. Connection to the Solartron FRA was by means of individually screened coaxial cables to the voltage high/low and current output/input terminals. Internal temperature of the samples was recorded using an embedded thermistor. System control and data logging were by means of a HP Vectra personal computer.

Table 2
Physical properties and oxide analysis of materials

	Microsilica	Fly ash	OPC
Physical properites			
Specific gravity	1.94	2.10	3.15
Surface area (m^2/kg)	15000 (BET)	330 (Blaine)	350 (Blaine)
Chemical analysis (%)			
SiO_2	85.9	48.9	20.68
Al_2O_3	1.5	27.4	4.83
Fe_2O_3	3.0	7.3	3.17
CaO	0.7	3.3	63.95
MgO	2.0	1.1	2.53
TiO_2	ND	1.2	ND
P_2O_5	ND	0.16	ND
SO_3	ND	0.47	2.80
K_2O	3.0	1.1	0.54
Na_2O	1.0	0.16	0.08

ND: not determined.

1.3. Calibration procedure

While the sample material is in the liquid state the cell impedance is low and, as the frequency of the applied field increases, the impedance of the connecting leads begins to dominate the measured values. This is a problem even when data were corrected using the internal nulling procedure available with the FRA. For this reason a procedure utilising open-circuit, short-circuit, and load calibration (using a precision resistor and capacitor) was performed at each test frequency; the technique on which this procedure is based is detailed elsewhere [23].

2. Discussion of results

The prime motivation of the work was to study and present data on these materials in the liquid state. As a consequence, measurements are presented 60 minutes after initial mixing with water. The calibration procedure ensured high-quality immittance data that hitherto has not been presented over the frequency range under consideration. Note that, for clarity, only every third data marker is highlighted on the response curves.

2.1. Impedance response: paste, mortar, and concrete

Fig. 3A–D present the Nyquist plots for paste, mortar, and concrete specimens. The specimens with plain OPC binder displays a typical two-region response comprising an

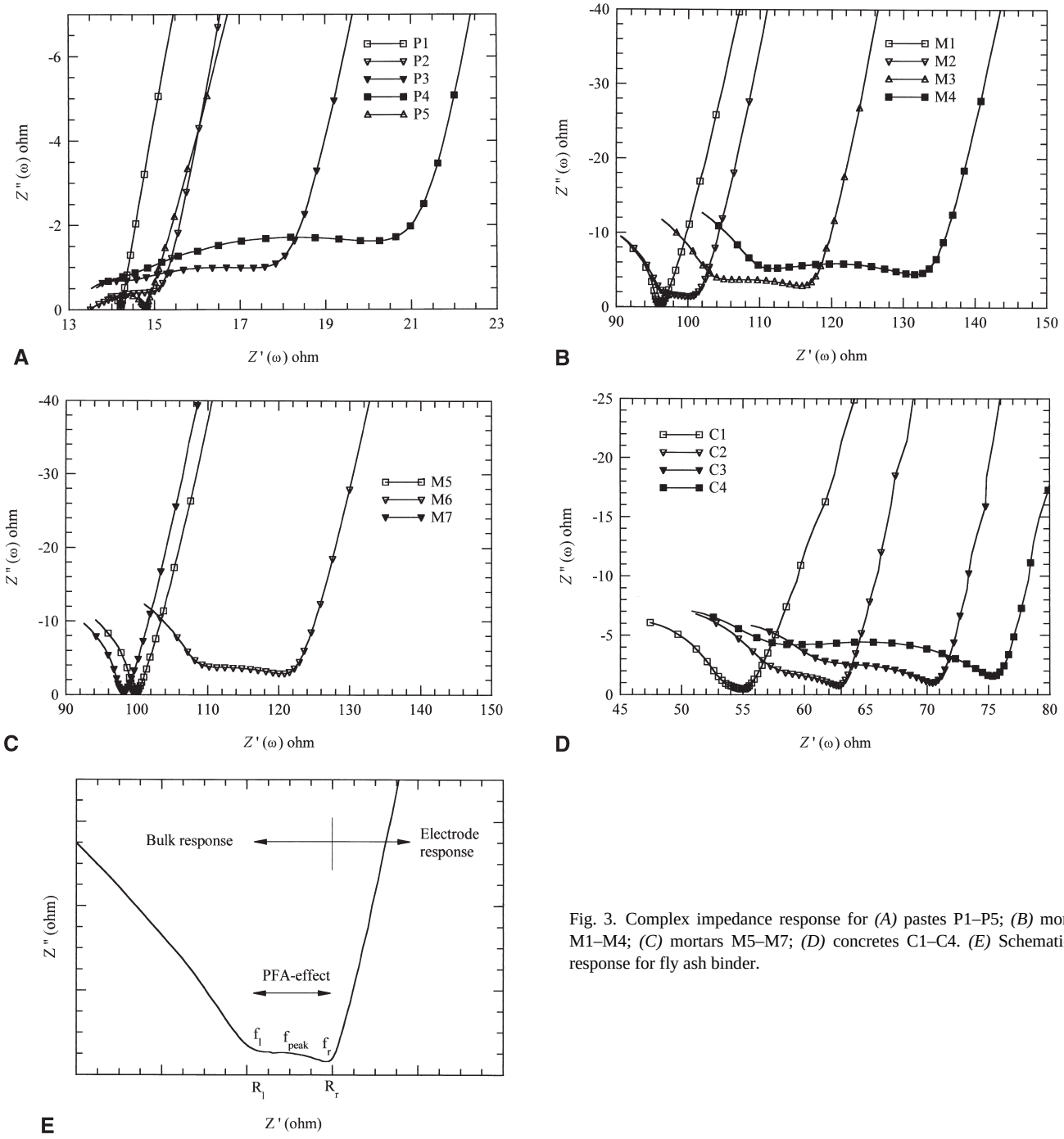

Fig. 3. Complex impedance response for *(A)* pastes P1–P5; *(B)* mortars M1–M4; *(C)* mortars M5–M7; *(D)* concretes C1–C4. *(E)* Schematic of response for fly ash binder.

electrode polarization "spur" forming the right-hand side of the "V"-shaped plot and the bulk sample arc forming the left-hand side of the overall response. This is also the case for the mortar samples with SRPC, OPC/MS, and SRPC/MS binders (Fig. 3C), although the impedance of the system is increased relative to the respective plain OPC binder. Regarding the increase in impedance for SRPC mortars, the reduced C_3A content of this cement will reduce ionic concentration in the interstitial aqueous phase, thereby increasing sample impedance. The replacement of OPC with MS is equivalent to increasing the volume fraction of nonconductive phase, thereby increasing impedance.

This set of figures clearly show the influence of the addition of FA and corroborates previous work, although in a more systematic manner. The FA responses display a Nyquist plot that is now characterised by three distinct zones: the electrode response, a plateau region due to inclusion FA, and a bulk arc. Regarding the latter, this loses clarity for the plain

Table 3
Frequency range over which fly ash plateau persists and the real (resistive) component at those frequencies

Mix	f_r (kHz)	f_1 (kHz)	f_{peak} (Khz)	R_r (ohms)	R_1 (ohms)
M1	8.94	—	—	96.25	—
M2	4.87	172	no peak observed	100.2	96.8
M3	1.25	205	52.4	115.9	105
M4	0.75	242	22.4	131.6	112
M5	8.90	—	—	99.8	—
M6	1.48	242	No peak observed	120.6	109.8
C1	2.08	—	—	55.0	—
C2	0.54	204	No peak observed	62.7	58
C3	0.27	242	No peak observed	70.4	63
C4	0.14	287	37.4	75.4	59

pastes and is more prominent in the mortars and concretes. In quantitative terms, the addition of FA results in a number of salient changes to the response, which are, in summary:

- The frequency range over which the plateau region persists is directly dependent on the FA content. With reference to Fig. 3E, Table 3 presents the frequency of applied field at the right- and left-hand extremes of the plateau region denoted, respectively, f_r, and f_l.
- The values of $Z'(\omega)$ at the frequencies f_r and f_l (denoted R_r and R_l) increase with increasing FA content and are presented in Table 3. The cementitious system becomes more resistive due to the inclusion of FA and is not dissimilar to MS in this respect.
- The plateau region has the appearance of a circular arc with its centre depressed below the real axis. Increasing the FA content results in better definition to the arc, and at the higher replacement levels a definite peak can be observed (at a frequency denoted f_{peak}, see Fig. 3E) and presented in Table 3.

2.2. Frequency dependence and relaxation processes

The dielectric constant and conductivity were de-imbedded from the impedance data using Eq. (2), and the resulting dispersion curves are presented in Fig. 4A–D and Fig. 5A–D, respectively. The impedance plots indicated that electrode effects are considerably reduced at frequencies in excess of 1 kHz; however, for the current study, conductivity and di-

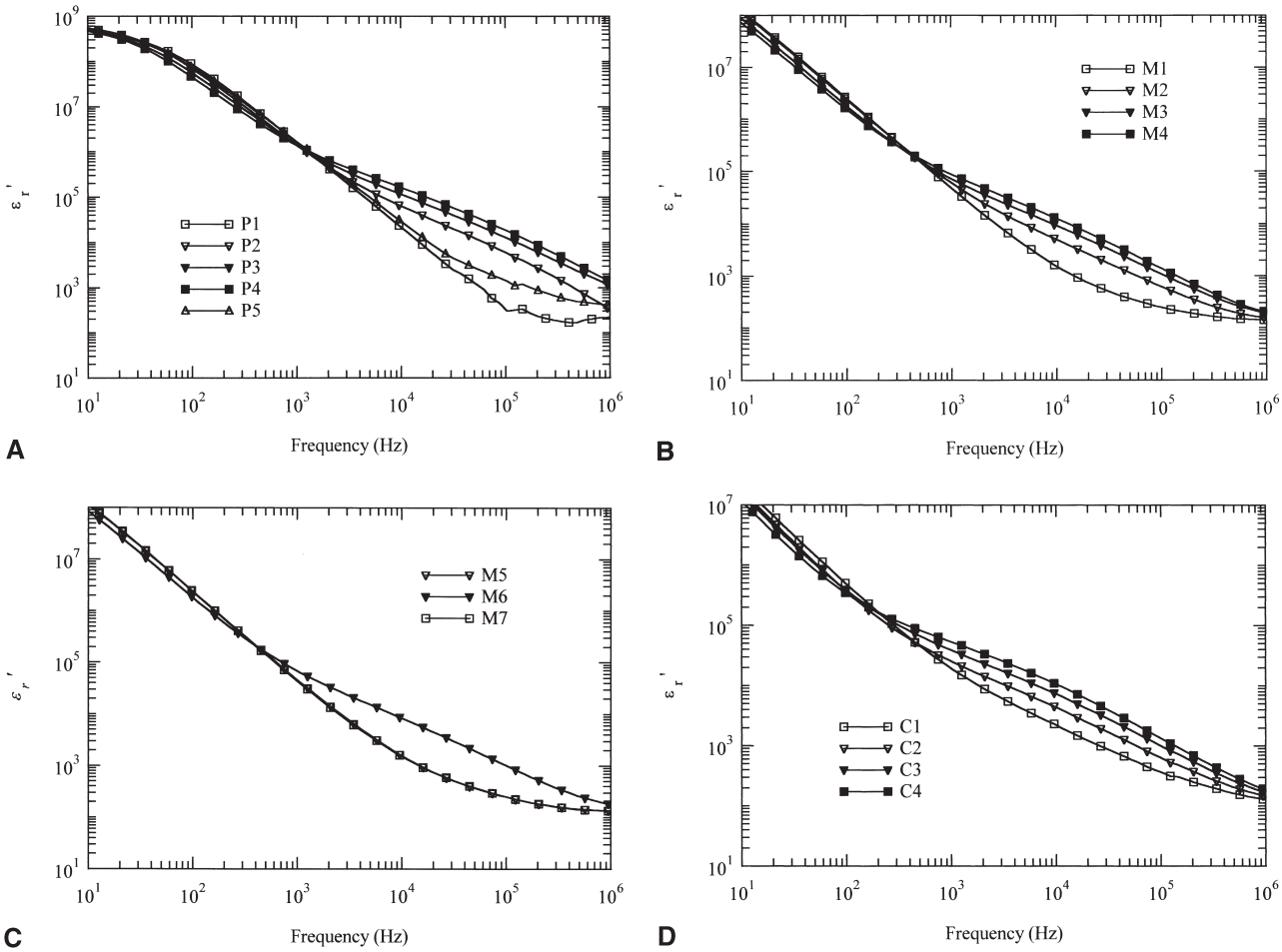

Fig. 4. Dielectric dispersion curves for *(A)* pastes P1–P5; *(B)* mortars M1–M4; *(C)* mortars M5–M7; *(D)* concretes C1–C4.

electric constant are presented over the full frequency range from 1 Hz to 1 MHz.

Considering the dielectric constant for pastes, mortars, and concretes (Fig. 4A–D), the decrease in this parameter with increasing frequency indicates a region of dispersion resulting from the relaxation of a polarization process within the system. If there existed a single, dominant relaxation process, the region of dispersion would, typically, be contained within one decade of frequency [22]. In fresh, cement-based systems, it is evident that relaxation occurs over several decades of frequency and is indicative of a spread of relaxation time constants. At frequencies below 1 kHz, the dielectric constant rises to extremely high values and would represent the increasing influence of the electrode/sample interfacial polarization effect. What is apparent for all mixtures is that, in comparison to the plain OPC mix, the inclusion of FA in the binder results in an enhancement of the bulk polarization processes, hence dielectric constant, at frequencies in excess of 1 kHz. This is particularly evident over the range from 10 kHz to 1 MHz, indicating the superposition of an added contribution to the dielectric response on that of the plain OPC. As the quantity of FA is increased, the magnitude of the dielectric enhancement increases, although the scale of this effect is masked by the logarithmic scale of the vertical axis.

Further supporting evidence for these conclusions can be obtained fron the conductivity dispersion curves shown in Fig. 5A–D. For the paste and mortar samples (Fig. 5A–C), the conductivity curves can be divided into two regions above and below 1 kHz (approximately). Below 1 kHz, and particularly over the region 1–100Hz, the sharp decrease in conductivity with decreasing frequency is as a result of the increasing contribution of electrode effects (as noted from the dielectric dispersion data). For the concrete samples (Fig. 5D), this low-frequency region is not as pronounced, because the cutoff frequency for electrode effects has been reduced (see f_r in Table 3).

At frequencies in excess of 1 kHz, there is a gradual rise in conductivity with increasing frequency; of particular interest is that as the FA replacement level increases, this dispersion in conductivity becomes more apparent. The frequency range over which the increase in conductivity occurs is the same as that for the dielectric enhancement effect of the FA. The increase in conductivity with increasing fre-

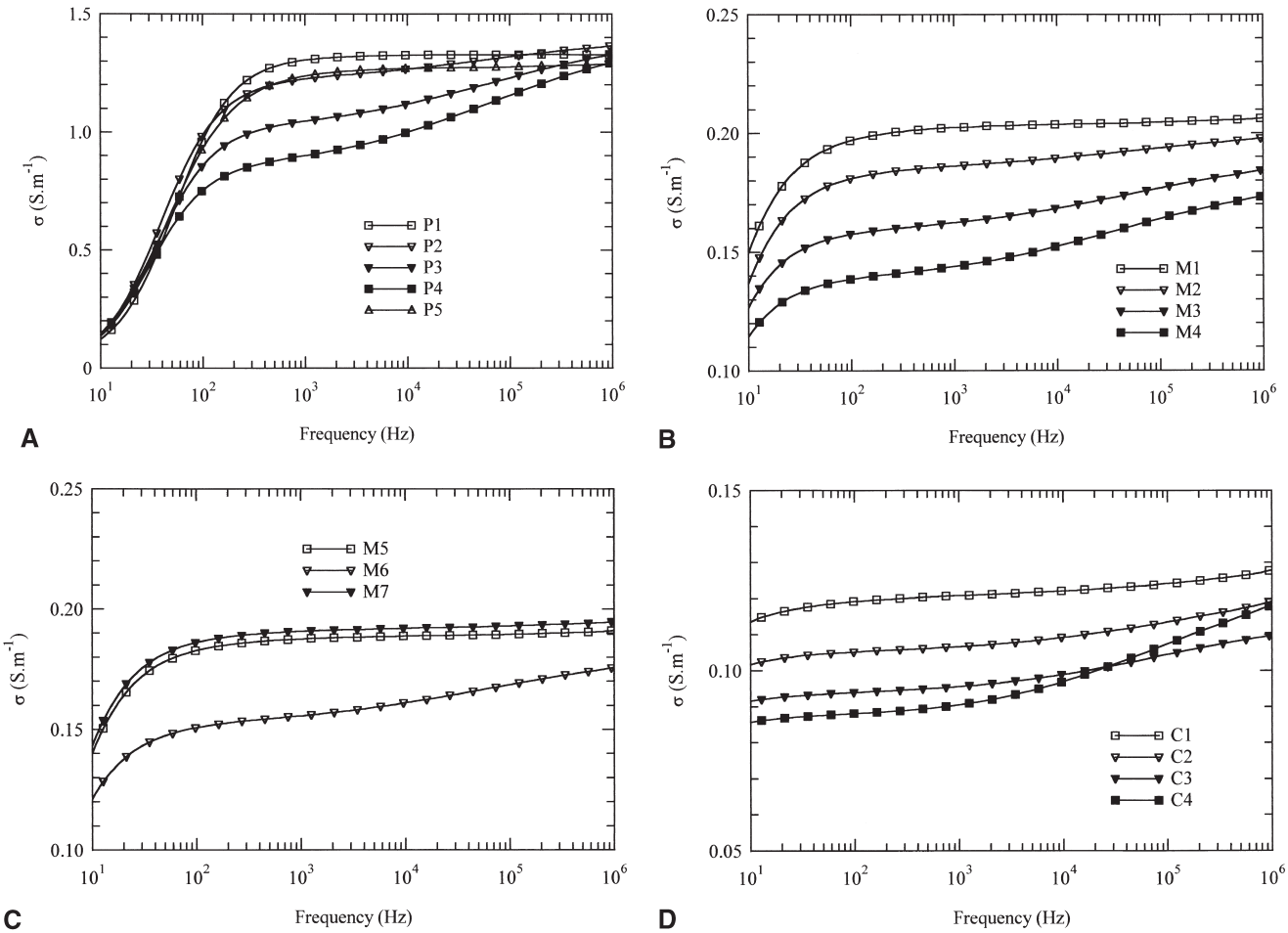

Fig. 5. Conductivity dispersion curves for *(A)* pastes P1–P5; *(B)* mortars M1–M4; *(C)* mortars M5–M7; *(D)* concretes C1–C4.

quency of applied field will be a direct result of relaxation of the polarization mechanism, which, in addition to ionic conduction effects, will contribute to loss processes [see Eqs. (4) and (5)]. The overall result will be an enhancement of measured conductivity.

In the first hour after gauging, little or no development of the eventual microstructure of the binder has taken place and the cementitious systems could be regarded as a suspension of binder particles and aggregate of various sizes surrounded by an interstitial aqueous electrolyte. Dielectric effects resulting from polarization processes [24] associated with the later microstructural features (i.e., the interconnected pore network) cannot be invoked to explain the electrical behaviour of the structurally simpler liquid system. On gauging, the interstitial aqueous phase provides a suitable environment for establishing an electrochemical double layer on the binder particles. Charges in the double layer are held in varying degrees of firmness: an inner layer held near the grain surface and a diffuse layer extending from the inner layer (at the plane of "slippage") to the bulk solution [25]. It could now be hypothesised that oscillation or movement of electrostatically held charges in sympathy with the applied electrical produces a double-layer polarization response, thereby inducing a large effective dipole (hence capacitance). This process is a low-frequency polarization mechanism and concentrated within the kHz range.

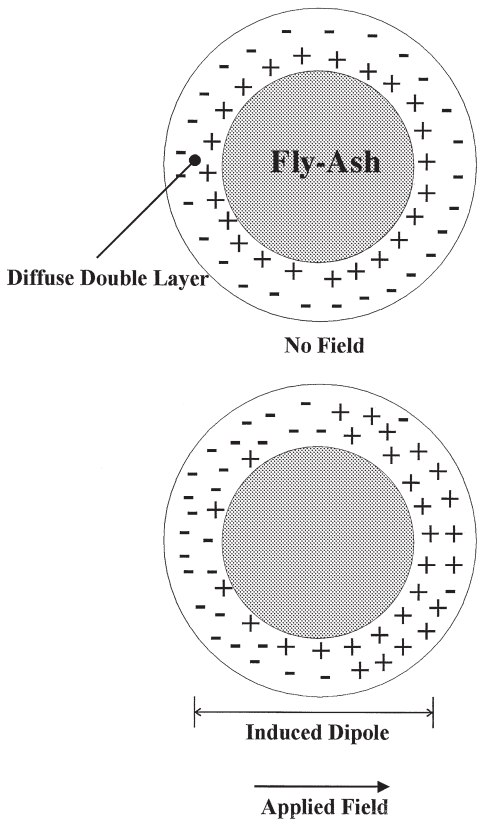

Fig. 6. Schematic diagram showing induced dipole moment due to double-layer polarization under the influence of an alternating electrical field.

The ease and range of movement of charges, together with the frequency of applied field, dictates the magnitude of the polarization response, which is quantified in the bulk capacitance of the system. To explain the enhanced double-layer polarization response of FA binders, although the size of the OPC and FA particles are similar (≈10–20 μm), consideration should be given to the distinctive spherical shape of the FA particle, schematically shown in Fig. 6. It is postulated that electrostatically held double-layer charges can oscillate more easily over the surface of the FA particle in response to the changing field than those on the more angular OPC particle. If this is the case, then the charges on the FA particle are more easily polarizable and ultimately results in a higher capacitance. It is also of interest to note that the zeta potential of FA is significantly different from that of plain OPC (the zeta potential being related to the extent of the double layer formed on the surface of the particle) [25–27].

Interestingly, although MS is also spherical in nature, it does not produce the distinctive impedance response. Dielectric enhancement is evident in the paste sample (Fig. 4A), although this has now shifted to a higher frequency range from 100 kHz to 1 MHz. Furthermore, this enhancement is approximately an order of magnitude lower than the FA binder at the same replacement level (10%). The enhancement for MS binders is not discernible when aggregate is added (Fig. 4C). MS is approximately two orders of magnitude smaller than FA, and the reason for the nonappearance of a plateau region could be a size effect, with a resulting reduction in the induced dipole moment effect (Fig. 6).

Consideration also should be given to the absolute values of dielectric constant for the cementitious systems presented, which are considerably higher than that of pure water (≈80). It is only at the upper end of the frequency range presented (1 MHz) that values reduce to ≈100, which is consistent with high-frequency data on fresh mortars and concretes [23]. Double-layer polarization processes on particle surfaces have been known to produce anomolously high dielectric constants; for example, it has been shown [28,29] that a suspension of polystyrene latex particles (of similar dimensions to FA particles) in potassium chloride solution display substantial dielectric enhancement at low frequencies. Double-layer polarization also has been invoked to account for the high dielectric constants obtained from porous sandstones impregnated with high-conductivity liquids [30–32].

The dielectric constant and conductivity of the systems containing aggregate are considerably lower than that of the plain binder and simply reflect the diluting effect of the aggregate.

2.3. Modeling of immittance response

It is possible to consider the impedance plot for the FA systems as three separate regions and then attempt an equivalent circuit analysis of each zone in turn, with each circuit

comprising a resistor in parallel with a constant phase element (CPE) given in Eq. (9), where:

$$\mathrm{CPE} = B_o(j\omega)^{-\alpha'} \tag{9}$$

and $\alpha' = (1–2\ \beta/\pi)$, β is the arc depression angle in radians ($0 < \beta < \pi/2$), and B_o is a constant. This is a reasonable approach with respect to that part of the response associated with the electrode-sample interfacial zone, as it results from an effect that is physically in series with the bulk impedance of the sample. However, we propose a different approach with respect to the two-region response for the FA binders.

Consider, for example, mortars M1 and M3 in Fig. 3B (0% and 25% FA replacement). Commercially available software was used (ZView) to perform an equivalent circuit analysis on the bulk response of these mortars. For M1, the low- and high-frequency intercept values on the real axis are, respectively, 95.6 and 70.1 ohms, the arc depression angle is 3.1°, and the frequency at the top of the arc was obtained as 18.7 MHz. This gave equivalent R-C circuit parameters of 25.5 ohms and 3.33×10^{-10} F, respectively. It is evident that, from the fitting process, the high-frequency intercept falls well short of the origin. For M3, the low- and high-frequency intercept values for the FA plateau region are, respectively, 124.8 and 89.4 ohms, the arc depression angle is 66.5°, and the frequency at the top of the arc was evaluated as 75.9 kHz. This gave equivalent R-C circuit parameters of 35.4 ohms and 2.36×10^{-8} F, respectively. The low- and high-frequency intercept values for the left-hand arc for M3 were, respectively, 105.7 and 28.2 ohms, and the arc depression angle was 28°. The frequency at the top of the bulk arc could not be evaluated from the software; hence, only the equivalent circuit resistance could be obtained (R = 77.5 ohms).

The view is taken here that the observed response should be sought at a more fundamental level in the dielectric properties of the material. The procedure adopted is to synthesize the impedance response by modelling its dielectric behaviour on the assumption that it is primarily the result of a single relaxation mechanism and as a modified (dispersed) Debye-type relative permittivity, inclusive of a low-frequency (or d.c.) conductivity component [see Eq. (6)].

Having established values for the parameters in Eq. (7) (ε_{rs}, $\varepsilon_{r\infty}$ τ_o, α), relative permittivity data can be generated for each frequency point of the original measurement data (in the range from 1 Hz to 1 MHz) and the results fed into Eqs. (2), (8a), and (8b), along with the cell constant, to produce dielectric constant, conductivity, and impedance data. As an example, the parameters values used in the synthesis of the relevant responses for M3 are presented in Table 4.

Table 4
Parameter values used for calculated immittance responses for mortar M3

DC conductivity	$\sigma_{dc} = 0.162$ S/m
Relaxation frequency ($\omega_0 = 2\pi f_o$)	$f_o = 2.9$ kHz
Dielectric constant: low-frequency limit	$\varepsilon_{rs} = 50{,}000$
Dielectric constant: high-frequency limit	$\varepsilon_{r\infty} = 60$
Dispersion spreading factor	$\alpha = 0.194$

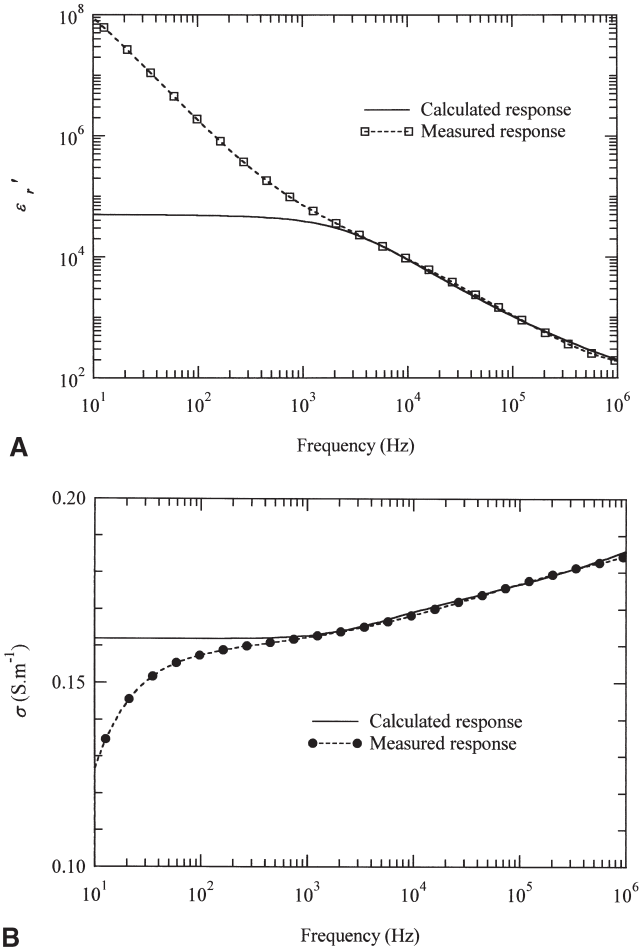

Fig. 7. *(A)* Dielectric constant and *(B)* conductivity dispersion curves measured and calculated using parameters in Table 4 for mortar M3.

Fig. 7 gives a comparison of the de-imbedded experimental dielectric constant (Fig. 7A) and conductivity (Fig. 7B) with the calculated response. Both of these curves show the good agreement between calculated and measured values, with the only notable discrepancies being below 1 kHz. Regarding the latter, at frequencies below about 1 kHz, the measured conductivity and dielectric constant start to attain very low and high values, respectively, and diverge from the simulated response. This is a result of the dominating influence of electrode effects on the measured data, which was not modelled in the theoretical response.

The impedance response obtained using these parameters is shown in comparison to the measured response in Fig. 8A over the full frequency range from 1 Hz to 1 MHz. Again, the fit between measured and calculated values is good, although in the case of the low-frequency data, electrode polarization effects were not accounted for in the synthesised response. The data between 1 kHz and 1 MHz also shows good agreement in frequency domain and impedance plots, with two regions clearly discernible in the calculated plot.

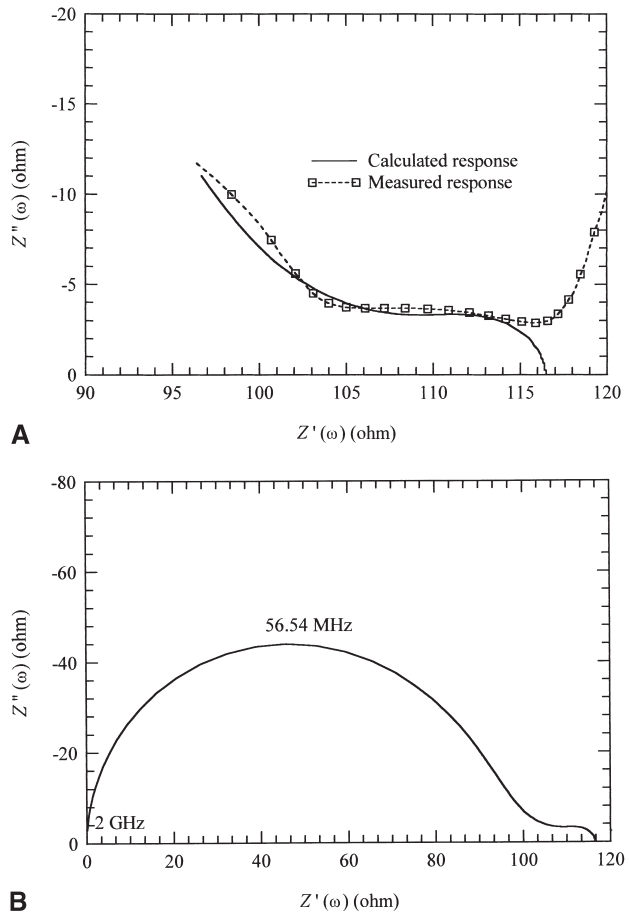

Fig. 8. *(A)* Measured and calculated complex impedance curve for mortar M3 using parameters in Table 4 and *(B)* calculated impedance plot to 10 GHz.

The traditional approach of analysing the two arc regions separately thus could give a false impression of the effects underlying the impedance response. In the present work, at the permittivity level, a single dispersion spreading parameter (α) affects both bulk arcs and the junction between them, such that the left-hand arc appears almost parabolic, or semielliptic (when viewed within the frequency constraints of the experimental data), and the middle arc appears to have a very large depression angle. In a more conventional impedance analysis using the CPE concept, two completely separate arc depression parameters (α') would be assigned to each of the arcs and the meaning of the response would be rather difficult to explain. The approach adopted allows two apparently unrelated effects to be attributed to a single cause, i.e., double-layer polarization, thereby simplifying interpretation of what is happening electrically within the material.

Finally, by extending the upper frequency limit for the synthesised data to 10^{10} Hz, the plot does project toward the origin, as would be expected from the impedance response of a genuine heterogeneous dielectric material. This is shown in Fig. 8B.

3. Conclusions

Measurements have been presented on the electrical response of a range of cementitious binders, with and without aggregate additions. Data were obtained while the material was in the liquid state and represents an area in which there is, currently, a dearth of information. Sample sizes were of realistic size and composition. A number of immittance parameters were presented and of particular interest were the dielectric constant and conductivity dispersion curves together with the complex impedance curves.

Electrical data were interpreted in terms of intrinsic bulk polarization and conduction processes. It was postulated that the region of dielectric and conductivity dispersion over the frequency range from 1 kHz to 1 MHz resulted from a double-layer relaxation process on the surface of binder particles. This manifested itself as a decrease in dielectric constant and a corresponding increase in conductivity with increasing frequency. The low-frequency conductivity (at approximately 1 kHz) was due to ionic conduction processes, whereas the elevation of conductivity above its low-frequency level resulted from relaxation of double-layer charges.

Of particular interest was the OPC/FA binder that produced a characteristic three-region response when presented in Nyquist format, with a mid-frequency plateau region developing between the low-frequency electrode arc and high-frequency bulk arc. The mid- and high-frequency regions constituted the bulk response. As an alternative to ascribing an equivalent electrical circuit to each of these regions and assigning a particular phenomenon to each region, it was shown that by considering the intrinsic bulk electrical parameters (dielectric constant, conductivity) together with the system relaxation frequency and dispersion spreading factor, a single polarization process could account for the impedance response of OPC/FA. This was highlighted by synthesizing the experimental results through the classical Debye equations. The inclusion of FA was seen to cause an increase in the polarizability of the system over the frequency range from 1 kHz to 1 MHz, which resulted in a dielectric enhancement.

Acknowledgments

The authors gratefully acknowledge the financial support of the Engineering and Physical Science Research Council, U.K. (Grant GR/K52430).

References

[1] W.J. McCarter, S. Garvin, Bouzid, J Mater Sci Lett 7 (1988) 1056–1057.
[2] W.J. McCarter, R. Brousseau, Cem Concr Res 20 (6) (1990) 891–900.
[3] K. Brantervik, G.A. Niklasson, Cem Concr Res 21 (4) (1991) 496–508.
[4] A. Berg, G.A. Niklasson, K. Brantervik, B. Hedberg, L.O. Nilsson, Solid State Commun 79 (1) (1991) 93–96.

[5] B.J. Christensen, T.O. Mason, H.M. Jennings, J Am Ceram Soc 75 (4) (1992) 939–945.
[6] A. Berg, G.A. Niklasson, K. Brantervik., B. Hedberg, L.O. Nilsson, J Appl Phys 71 (12) (1992) 5897–5903.
[7] P. Gu, P. Xie, J.J. Beaudoin, R. Brousseau, Cem Concr Res 22 (5) (1992) 833–840.
[8] P. Gu, P. Xie, J.J. Beaudoin, R. Brousseau, Cem Concr Res 23 (1) (1993) 157–168.
[9] P. Gu, P. Xie, J.J. Beaudoin, R. Brousseau, Cem Concr Res 23 (2) (1993) 359–367.
[10] Z. Xu, P. Gu, P. Xie, J.J. Beaudoin, Cem Concr Res 23 (3) (1993) 531–540.
[11] Z . Xu, P. Gu, P. Xie, J.J. Beaudoin, Cem Concr Res 23 (4) (1993) 853–862.
[12] R.T. Coverdale, E.J. Garboczi, H.M. Jennings, B.J. Christensen, T.O. Mason, J Am Ceram Soc 76 (6) (1993) 1153–1160.
[13] R.T. Coverdale, B.J. Christensen, T.O. Mason, H.M. Jennings, E.J. Garboczi, J Mater Sci 29 (1994) 4984–4992.
[14] D.E. MacPhee, D.C. Sinclair, S.L. Stubbs, J Mater Sci Lett 15 (1996) 1566–1568.
[15] M. Keddam, H. Takenouti, X.R. Novoa, C. Andrade, C. Alonso, Cem Concr Res 27 (8) (1997) 1191–1201.
[16] G. Ping, J.J. Beaudoin, Adv Cem Res 9 (33) (1997) 1–8.
[17] C.A. Scuderi, T.O. Mason, H.M. Jennings, J Mater Sci 26 (1991) 349–353.
[18] W.J. McCarter, Cem Concr Res 24 (6) (1994) 1097–1110.
[19] W.J. McCarter, J Mater Sci 31 (1996) 6258–6292.
[20] W.J. McCarter, G. Starrs, J Mater Sci Lett 16 (1997) 605–607.
[21] J.R. Macdonald, J Non-Crystal Solids 16 (2/3) (1996) 83–110.
[22] J.B. Hasted, Aqueous Dielectrics, Chapman and Hall, London, 1973.
[23] G. Starrs, Measurement of the Electrical Properties of concrete at radio frequencies, PhD Thesis, Napier University, Edinburgh, Scotland, 1994.
[24] W.J. McCarter, H. Ezirim, Adv Cem Res 10 (2) (1998) 57–66.
[25] E. Nagele, Cem Concr Res 15 (3) (1985) 453–462.
[26] E. Nagele, Cem Concr Res 16 (6) (1986) 853–863.
[27] E. Nagele, Cem Concr Res 17 (4) (1987) 573–580.
[28] H.P Schwan, G. Schwarz, J. Maczuk, H. Pauly, J Phys Chem 66 (1962) 2626–2635.
[29] G, Schwarz, J Phys Chem 66 (1962) 2636–2642.
[30] W.C. Chew, P.N. Sen, J Chem Phys 77 (9) (1982) 4683–4693.
[31] P.N. Sen, W.C. Chew, J Microwave Power 18 (1) (1983) 95–105.
[32] B. Nettelblad, G.A. Niklasson, J Mater Sci 32 (1997) 3783–3800.